Carbon 152 (2019) 363–371

Contents lists available at ScienceDirect

Carbon

journal homepage: www.elsevier.com/locate/carbon

Elastic carbon dot/polymer films for fluorescent tensile sensing and mechano-optical tuning

Nitzan Shauloff [a], Sagarika Bhattacharya [a], Raz Jelinek [a, b, *]

[a] Department of Chemistry, Ben Gurion University of the Negev, Beer Sheva, 84105, Israel
[b] Ilse Katz Institute for Nanotechnology, Ben Gurion University of the Negev, Beer Sheva, 84105, Israel

ARTICLE INFO

Article history:
Received 22 February 2019
Received in revised form
8 May 2019
Accepted 8 June 2019
Available online 11 June 2019

Keywords:
Carbon dots
Tensile strain sensing
Mechano-responsive polymers
Stress sensing

ABSTRACT

Development of simple, readily-applicable sensors for mechanical deformation of polymers is highly sought albeit a formidable task. Here we demonstrate that composite films comprising carbon dots (C-dots) embedded in an elastic polymer host allow fluorescence-based quantitative determination of tensile modulation. Film stretching induced both blue shift in the C-dots' fluorescence peak positions and dramatic increase in fluorescence intensities. The phenomenon was demonstrated for different C-dots exhibiting distinct fluorescence emissions (e.g. colors). Importantly, the C-dot/polymer fluorescence intensity could be quantitatively correlated to tensile parameters, specifically film stress and strain. The direct correlation is ascribed to stretch-induced modulation of the average distances among the polymer-embedded C-dots and concomitant modification of aggregation-induced self-quenching. We further exploited the tensile-dependent fluorescence modulation of the C-dot/polymer system to construct a tunable-intensity white light emitter, opening the way to innovative mechanically-tuned optical device.
© 2019 Elsevier Ltd. All rights reserved.

1. Introduction

Mechano-responsive polymer composites have attracted significant scientific and technological interest in recent years, due to their use in varied devices and applications, including Wearable Devices for Monitoring Physiological Markers [1,2], Self-Healing Materials [3,4], mechanically-activated drug-delivery systems [5]. electro-optical modulators [6–9], and others. The development of new shape-deformable polymeric materials has progressed hand in hand with introducing new analytical platforms for assessing mechanical modulation [10].Indeed, polymer-deforming sensors have been employed in applications such as tamper-proof packaging [11], health monitoring [12],and wearable electronic devices for monitoring human motion [13–16]. Stress and strain are the fundamental parameters describing the physical impact upon mechano-responsive polymers, and as such varied techniques have been developed to evaluate these parameters. Reported stress/strain sensors have relied upon varied techniques, such as recording electrical signals upon mechanical force application using extensometers and piezoelectric sensors [17], application of Raman spectroscopy [18], and photo-elasticity measurements [19]. Such methods, however, are limited by measurement areas, are often experimentally complex, or are not amenable for real-time analyses [20].

Polymer-embedded optical sensing has gained particular interest as a simple visual means for assessing mechanical deformation [21]. In general, optical tensile sensing of mechano-responsive polymers has been carried out through embedding dyes [22], functional molecules [23], metallic and inorganic nanoparticles [24,25], or excimers [26] within the polymeric matrix undergoing shape changes. These composite materials change their light absorbance or fluorescence emission in response to mechanical transformations [3,27]. Significant hurdles, however, have been encountered for wider applicability of these sensing schemes, primarily due to the mostly complex synthetic schemes, lack of quantitative correlation with actual mechanical parameters (such as stress/strain), and confined polymer areas analyzed.

Carbon dots (C-dots), nanometer-scale carbonaceous nanoparticles exhibiting unique physico-chemical properties, have emerged in recent years as a powerful fluorescent sensing platform, exhibiting diverse applications in chemo- and bio-sensing [28–31], imaging [32–34], and photonics [35].C-dots exhibit intriguing excitation-dependent fluorescence properties, determined in large part by the surface properties of the particles, particularly the

* Corresponding author. Department of Chemistry, Ben Gurion University of the Negev, Beer Sheva, 84105, Israel.
E-mail address: razj@bgu.ac.il (R. Jelinek).

https://doi.org/10.1016/j.carbon.2019.06.046
0008-6223/© 2019 Elsevier Ltd. All rights reserved.

functional units displayed upon the carbonaceous nanoparticles' surface [36–39]. Notably, C-dots can be readily synthesized from diverse carbon-containing reagents which allow tailoring their chemical and optical properties [40].

Similar to other fluorescent nanoparticles, C-dots' fluorescence is usually quenched when the particles are in close proximity to each other [41]. This feature has generally limited applicability of C-dots in solid-phase materials, and varied strategies have been introduced to ameliorate aggregation-induced quenching of C-dots, usually focusing on their incorporation and immobilization in host matrixes which maintain distance among the particles [42,43]. Here, we introduce a new C-dot/polymer composite in which the distance-dependent fluorescence properties of the C-dots are exploited for tensile sensing. This system is designed to provide an optical means for stress-strain determination through exploiting the C-dots' self-quenching properties. Remarkably, we show that the fluorescence shifts and intensity of different C-dots embedded in a transparent elastic polymer undergo significant tensile-dependent transformations. Importantly, we show that the fluorescence emissions of the C-dots were correlated to the stress and strains of the composite films, making possible optical determination of the tensile properties. Finally, we employ the tensile-dependent fluorescence strategy for creating an innovative mechanically-tuned light emitter.

2. Experimental section

2.1. Materials

Cetylpyridinium chloride monohydrate (CPC), polyvinyl butyral (PVB), and polyvinyl alcohol (PVA) were purchased from Sigma-Aldrich Chemicals, Jerusalem, Israel.1,5-Diaminoanthraquinone (Daaq)was purchased from Alfa-Aesar, Heysham, England. chloroform, Hydrochloric acid (HCl), ethanol (EeOH) and dichloromethane (CH2Cl2), Sodium Oxide (NaOH) were purchased from Bio-lab Itd. Hayetzira, Jerusalem, Israel. Teflon plates were custom-made. Single-side polished and heavily doped p-type Si wafers were purchased from Sil'tronix Silicon Technologies, Archamps, France.0.22 Non-Sterile Millex® Syringe Filters with Hydrophilic PTFE Membrane were purchased from Merck, Darmstadt, Germany.Water used in the experiments was doubly purified by a Barnstead D7382 water purification system (Barnstead Thermolyne, Dubuque, IA), at a resistivity of 18.3 MΩ cm. All reagents of analytical reagent grade or above were used as received without further purification.

2.2. Synthesis of CPC-C-dots

Synthesis of the CPC-C-dots was based upon reported procedures for construction of C-dots soluble in organic solvents [44]. Briefly, 150 mg of CPC was dissolved in 9 ml of deionized water. 360 mg of NaOH dissolved in 1 ml of deionized water was then added to the CPC solution which turned immediately yellow. The solution was mixed for 12 h and let to stand at room temperature without applying any external energy until turning brown. The solution was subsequently neutralized with 5% HCl solution, 10 ml of dichloromethane were added and the resultant C-dots were extracted from the bottom of the organic layer. The extracted solution was centrifuged twice for 5 min at 14,000 rpm, removing the larger aggregates. Dialysis was then performed in chloroform for 2 days using dialysis tubing (Avg. flat width 9 mm (0.35 in.), MWCO 2000). An intense brown powder was obtained after evaporation of the organic solvent (45 mg).

2.3. Synthesis of Daaq-C-dots

50 mg of Daaq were heated in 10 mL EtOH solvent at 200 °C for 24 h in a Teflon autoclave. The solution became brown red.The extracted solution was then centrifuged twice for 5 min at 14,000 rpm for separation of larger aggregates. Ethanol was subsequently evaporated and the dry content was dissolved in chloroform and placed for dialysis for 2 days (Avg. flat width 9 mm (0.35 in.) dialysis tubing, MWCO 2000). An intense black color powder was obtained after evaporation of the organic solvent (8.3 mg).

2.4. Preparation of C-dot/PVB composite film

500 mg of PVB powder (with 6% PVA) were dissolved in 8 ml of chloroform and sonicated for 25 min to form homogeneous solution. 20 mg of C-dot were dissolved in 2 ml chloroform and added to the polymer solution, mixed for 5 min using a Vortex to get uniform dispersion. the mixed solution was poured into a Bone shape Teflon plate (depth of 0.5 cm and surface of 35 cm^2) in a fume hood for the evaporation of chloroform, obtaining the C-dot/PVB composite film.

2.5. Characterization

Fluorescence spectroscopy: Fluorescence emission spectra of the different C-dots solution and the C-dot/PVB film were recorded on an FL920 spectro-fluorimeter (Edinburgh Instruments, Livingston, UK). Fluorescence emission spectra were acquired in the range of 400–700 nm with different excitation. Measuring the fluorescence after incorporation of the C-dots with PVB polymer creating the fluorescent films was carried out using a suitable stand for solid state materials. The fluorescence was measured at a 90° angle relative to the excitation light. This geometry is used instead of placing the sensor at the line of the excitation light at a 180° angle in order to avoid interference of the transmitted excitation light [45]. **High resolution transmission electron microscopy (HR-TEM):** A drop of C-dot solution was placed upon a graphene-coated copper grid and HR-TEM images were observed on a 200 kV JEOL JEM-2100F microscope (Japan), The sample was dried for 12 h prior to measurements. **Transmission electron microscopy** (**TEM**): images were observed on a 200 kV Thermo-Fisher Scientific Talos F200C with the same graphene-coated copper grids. **Atomic force microscopy (AFM):** AFM images were collected in AC-mode (tapping mode), with a Cypher-ES, asylum research (oxford instrument) model, using an AC 160 TS (olympus) probe, with a tip radius of 9 nm and a force constant of approximately 26 Nm−1. The C-dots solution (4 mg/ml) were mixed using a Vortex for 5 min then deposited onto hot silicon wafers wormed to 80 °C for fast evaporation (avoiding aggregates formation) [46]. **X-ray photoelectron spectroscopy (XPS):** Concentrated solutions of C-dots were drop-casted on silicon wafers and measurements were performed using an X-ray photoelectron spectrometer ESCALAB 250 ultrahigh vacuum ($1 \times 10-9$ bar) apparatus with an AlKα X-ray source and a monochromator. The beam diameter of was 500 μm and with pass energy (PE) of 150 eV survey spectra were recorded, while for high energy resolution spectra the recorded pass energy (PE) was 20 eV. The AVANTGE program was used to process the XPS results. **Fourier transform-infrared (FT-IR):** FTIR spectra were recorded on a Nicolet FTIR spectrometer (6700 FTIR spectrometer), using the attenuated total reflectance (ATR) technique with a diamond crystal, collecting data with clean crystal as a background. For each sample, a reference spectrum was first acquired from a clean crystal then the Spectra of dry samples were recorded by putting few mgs of dried sample. Analysis was carried out using Omnic (Nicolet, Madison, WI, USA) software. **Differential scanning calorimetry**

(DSC): Experiments were carried out on a DSC Mettler Toledo model DSC 823 (Switzerland). Heating rates of 20 °C/minute were used in a nitrogen atmosphere. ζ-Potential: ζ-potential was measured by Zetasizer (Zetasizer Nano ZS, Malvern, Worcestershire, UK) on 1 mL solutions of the CPC C-dots, at a concentration of 0.1 mg/ml. A Malvern DTS 1070 disposable capillary cuvette was used. Results are given as the means of four replicates [47]. **Ultraviolet visible (UV–vis) spectroscopy:** UV–vis spectra were acquired on a Thermo Scientific Evolution 220 spectrophotometer. All absorbance measurements were performed using 1-cm cells in water as dispersive medium. Confocal microscopy: films images were taken by CLSM (Plan-Apochromat 20×/0.8 M27, Zeiss LSM880, Germany), using 10 μm sectioning of paraffin-embedded polymers (Microtome instrument was used for sectioning) [48].

2.6. Tensile test

The tensile analyses were conducted in accordance with the ASTM D882-09 standard using a Zwick 1445 tensile instrument (Zwick Roell AG, Germany) [49]. All tests were conducted under standard laboratory conditions (temperature = 23 ± 2 °C; relative humidity = 50 ± 5%) on dry samples. Two crosshead speeds used for the testing with 20 mm/min rate and gauge length of 50 mm with the testing speed of 500 mm/min. The test control and data acquisition were achieved using Zwick 1445 computer software. In order to measure the fluorescence intensity at a specific strain value, the tensile measurement was paused at a given strain value and the film was then transferred to a fluorometer wherein the fluorescence intensity in the center of the film was measured at a set excitation wavelength. The film was then transferred back to the tensile instrument for further stretching.

2.7. Fabrication of mixed C-dot/PVB films

500 mg PVB powder was dissolved in 8 ml of chloroform and sonicated for 25 min. 16 mg of Daaq C-dots and 4 mg of CPC C-dot were mixed in 2 ml chloroform (ratio of 8:2), added to the polymer solution, mixed for 5 min using a Vortex to get a uniform dispersion. The mixed solution was poured into a Teflon plate in a fume hood, yielding the C-dot/PVB composite film after the evaporation of chloroform, appearing in an orange color. Light emission of the film was measured in an integrating sphere using a 410 nm LED; specifically, the film was placed between the optic fibre and the blue LED, generating white light.

3. Results and discussion

3.1. Experimental strategy

Fig. 1 outlines the fabrication and operation principle of the stretch-sensitive C-dot/polymer films. Construction of the C-dot/polymer composite films is depicted in Fig. 1A. We began with synthesis of the C-dots, prepared from the carbonaceous precursors cetylpyridinium chloride (CPC, yielding green C-dots) [44], and 1,5-Diaminoanthraquinone (Daaq) which generated red C-dots. The C-dots were interspersed in an organic solvent with polyvinyl butyral (PVB), a widely-used thermoplastic polymer that can mold at room temperature into stretchable transparent films [50]. Notably, due to the mild synthesis conditions (particularly low temperature), C-dots retain precursors' functional residues upon their surfaces [51]; in the systems presented here, both CPC-C-dots and Daaq-C-dots displayed the substituted aromatic residues, amine moieties, in addition to carbonyl and hydroxyl units on their surfaces (Fig. 1A). As depicted in Fig. 1A, polar residues at the C-dots' surfaces enable C-dot immobilization within the PVB host matrix through hydrogen bond formation.

The cartoon in Fig. 1B illustrates the novel phenomenon underlying the stretch-sensing properties of the C-dot/PVB films. The as-prepared C-dot/PVB composite film comprised of 4% C-dots by weight (Figs. 4C and SI). In this concentration, the embedded C-dots experience two opposing effects. On the one hand the solid polymer host matrix blocks aggregation of the C-dots and concomitant fluorescence quenching [52]. On the other hand, the proximity of the C-dots to one another likely to cause a certain tuning of the C-dots' fluorescence emission akin to aggregation-induced quenching [53]. Consequently, as shown in Fig. 1B, the *un-stretched* C-dot/PVB film exhibits low fluorescence emission. However, when the film is stretched, the distances between the C-dots increase, thereby giving rise to *lesser* fluorescence quenching and more pronounced emission. In parallel, the stretched PVB network modified the chemical environment of the embedded C-dots, giving rise to a *shift* in the position of the emission peak (Fig. 1B).

3.2. Characterization of the carbon-dot/PVB composite films

Fig. 2 depicts microscopy and spectroscopy characterization of the CPC-C-dots. The representative atomic force microscopy (AFM) image in Fig. 2A shows relatively uniform spherical C-dots, further reflected in the magnified region (Fig. 2A, inset). Particle size analysis indicates that the C-dots exhibited diameters of 7.4 ± 0.2 nm (Figs. 1A and SI). The high-resolution transmission electron microscopy (HR-TEM) image in Fig. 2B confirms the crystalline graphitic nature of the C-dots' carbon cores [54], displaying well-resolved lattice spacing of 0.21 nm and 0.33 nm, corresponding to the (100) and (002) lattice planes of graphite, respectively [30,55]. The transmission electron microscopy (TEM) image in Figs. 1B and SI revealing the uniform spherical nanoparticles. The excitation-dependent fluorescence spectra of the CPC-C-dots (Figs. 1C and SI) exhibit a maximal emission peak at 538 nm (λ_{ex} = 400 nm) accounting for the green colour of the C-dots. The excitation-dependent fluorescence spectra of the Daaq-C-dots (Figs. 2C and SI) exhibit a maximal emission peak at 600 nm (λ_{ex} = 480 nm) accounting for the red colour of the C-dots.

The Fourier transform infrared (FTIR) spectra of the CPC precursor and CPC-C-dots in Fig. 2C illuminate the functional units retained in C-dots (Fig. 2C). Specifically, the FTIR peaks between 1330 and 1380 cm-1 are assigned to C–N bonds, the signals at 1460-1520 cm-1 correspond to aliphatic carbons, while the FTIR peak at 1630 cm-1 is ascribed to C=N vibration bond of the pyridinium rings upon the carbon dot surface [44]. The intensity variations between the CPC precursor and the CPC-C-dots apparent in Fig. 2C are indicative to C-dot formation [56]. The deconvoluted nitrogen 1s x-ray photoelectron spectrum (XPS) of the CPC-C-dots in Fig. 2D corroborates the FTIR data, confirming retaining of the CPC functional units upon the C-dot surface. Specifically, the spectrum shows peaks at 399.1, 400.0, and 401.7 eV, are assigned to pyridine-N (C=N), pyrrolic-N (C–N),and N–H groups, respectively [44,57]. Zeta potential analysis (Tables 1 and SI) confirms the abundance of positively charged pyridinium units on the surface of the CPC-C-dots. Spectroscopic and microscopic characterization of the Daaq-C-dots is provided in Figs. 2 and SI. UV–vis spectra of CPC-C-dots and Daaq-C-dots (Figs. 3 and SI) confirmed the transformation of the precursors into the C-dot assemblies.

C-dot/PVB composite films were fabricated by simple mixing of the C-dots and polymer solutions, aided by a brief sonication and followed by evaporation of the organic solvent (Fig. 1). Fig. 3 presents spectroscopic and thermodynamic experiments examining the mutual effects upon both CPC-C-dot and PVB constituents in the mixed C-dot/PVB film. While the CPC-C-dots retained the typical excitation-dependent emission spectra even after

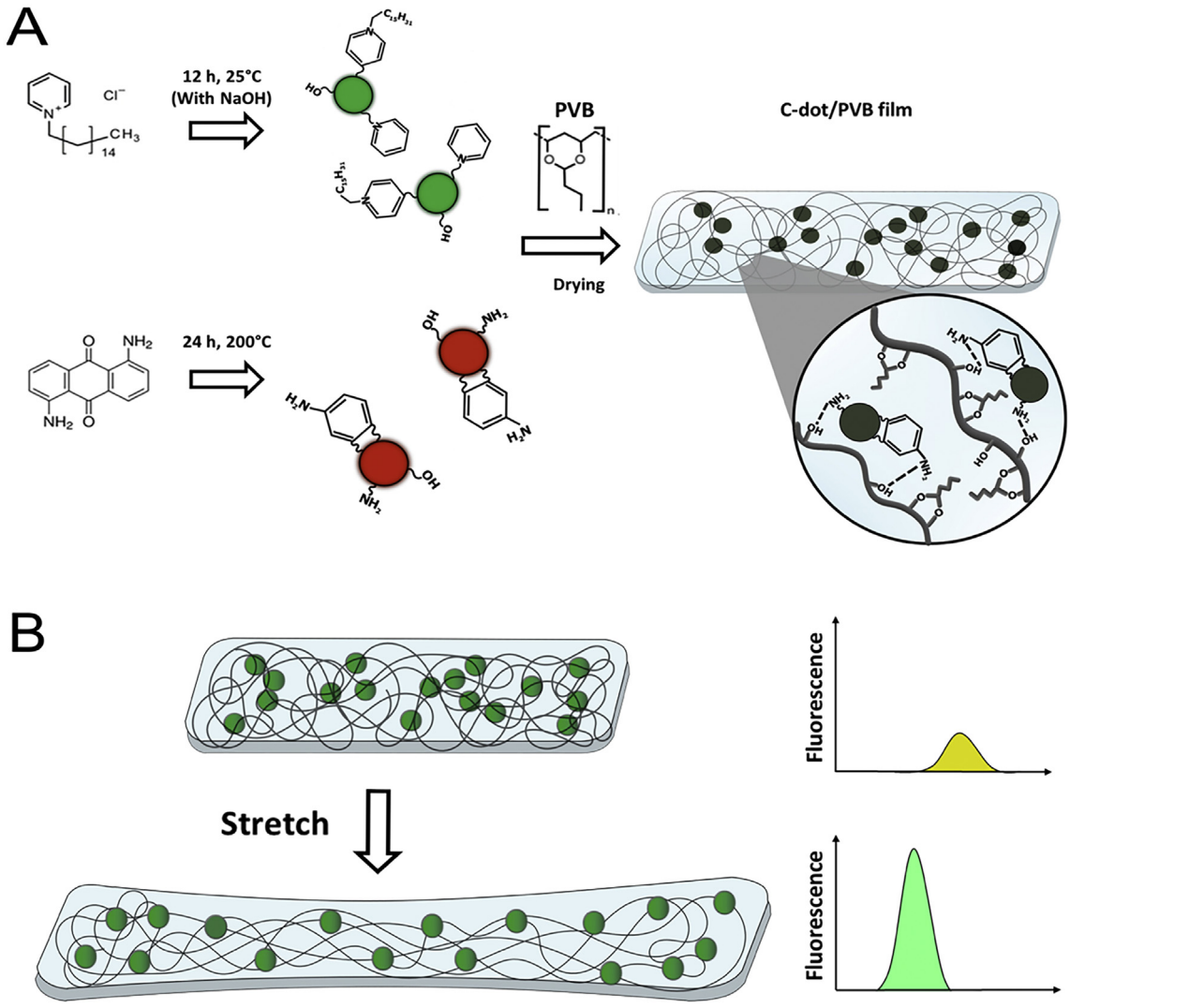

Fig. 1. Preparation of the elastic carbon-dot/polymer films and their stretch-dependent fluorescence properties. (**A**) Fabrication of the films using either green C-dots prepared from the CPC precursor (top row), or red C-dots from Daaq as the carbonaceous precursor (bottom row). The C-dots are immobilized within the PVB polymer framework through hydrogen bonding. (**B**) Fluorescent tensile sensing in the C-dot/PVB films. Both the position and intensity of the fluorescent peak change due the film stretching which modulates the average distance among the fluorescent C-dots. (A colour version of this figure can be viewed online.)

incorporation within the PVB matrix (Figs. 4A and SI), This phenomenon was also apparent in case of the Daaq-C-dots/PVB film (Figs. 4B and SI). Importantly, the C-dot/PVB composites retained excellent transparency to incoming light (Figs. 5 and SI). An additional confocal fluorescence microscopy experiment carried out on films' cross-sections confirmed encapsulation of the C-dots in the entire film volume (Figs. 6 and SI).

Fig. 3A reveals that a significant blue shift for the highest emission peak, from around 550 to 530 nm (excitation at 400 nm) occurred upon film formation. This result likely reflects significant interactions of the CPC-C-dots with the PVB matrix, altering their chemical environments and corresponding fluorescence emission position [58]. Indeed, the blue shift of the CPC-C-dots in the composite film is probably due to hydrogen bonding between polar units at the C-dots' surface and hydroxyl groups within the PVB framework [59,60]. Supporting this interpretation is the observation of similar blue emission shifts upon placing the C-dots in polar vs. non-polar solvents (Figs. 7 and SI).

While the fluorescence results in Fig. 3A attest to the impact of PVB incorporation upon the properties of the CPC-C-dots, we also tested the reciprocal effect of the embedded C-dots upon the PVB host (Fig. 3B). The differential scanning calorimetry (DSC) thermograms in Fig. 3B show the glass transition (Tg) of PVB [61], prior to, and after incorporation of the CPC-C-dots. Importantly, Fig. 3B demonstrates a significant decrease in Tg, by almost 6 °C, in the CPC-C-dot/PVB composite compared to PVB alone. A similar result was apparent in case of DAAQ-C-dots (Figs. 8 and SI). The lower Tg in the CPC-C-dot/PVB composite is ascribed to interference of the embedded C-dots in the gyration radius of the polymer chains, thereby increasing the free volume [62,63]. A similar thermodynamic effect has been reported in other nanomaterial/polymer composites [64].Together, the fluorescence spectroscopy and DSC data in Fig. 3 point to significant interactions between the C-dot guests and PVB host in the C-dot/PVB films.

3.3. Fluorescence sensing of carbon-dot/PVB film stretching

The thrust of this study was to investigate the relationship between the fluorescence properties of the C-dot/PVB films and their mechanical deformations. Indeed, Figs. 4 and 5 demonstrate remarkable correlations between the fluorescence emission of the C-dot/PVB composites and mechanical stretching of the films. Fig. 4

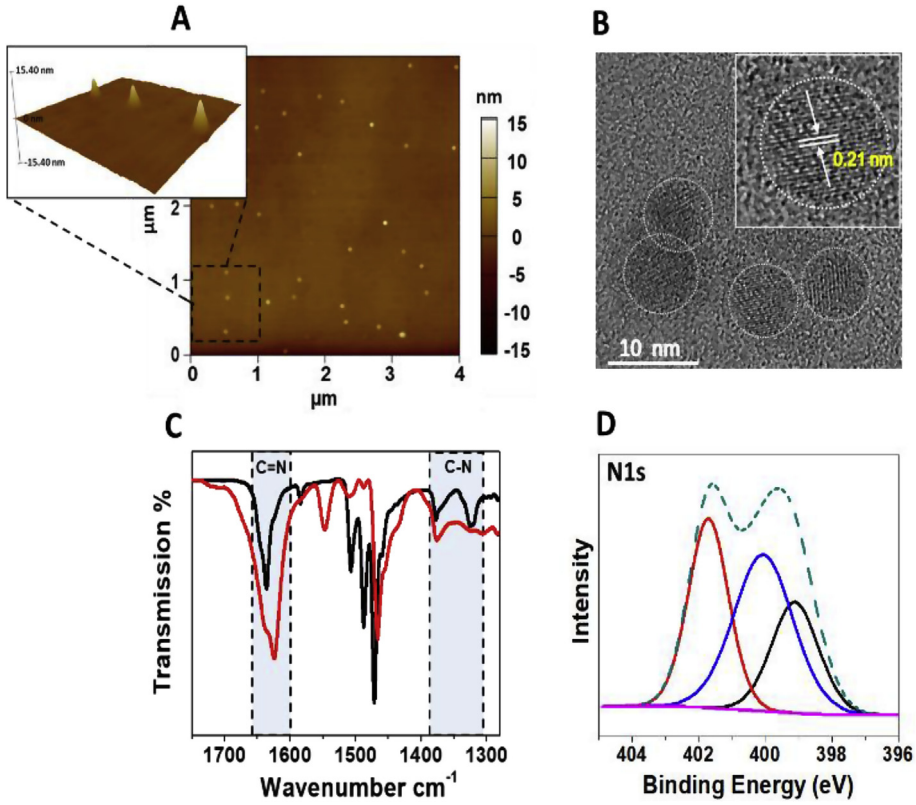

Fig. 2. Characterization of the carbon dots. (**A**) Representative atomic force microscopy (AFM) image of 2 mg/ml CPC-C-dots in Chloroform solution on a SiO2 substrate; a 1 × 1 μm cropped area is further magnified. (**B**) High resolution transmission electron microscopy (HRTEM) image of CPC-C-dots showing the graphitic crystalline lattice planes. The magnified image highlights the graphite lattice spacing of 0.21 nm. (**C**) Fourier transform infrared (FTIR) spectra of the CPC precursor (black) and CPC-C-dots (red). (**D**) N 1s X-ray photoelectron spectrum (XPS) of CPC-C-dots. (A colour version of this figure can be viewed online.)

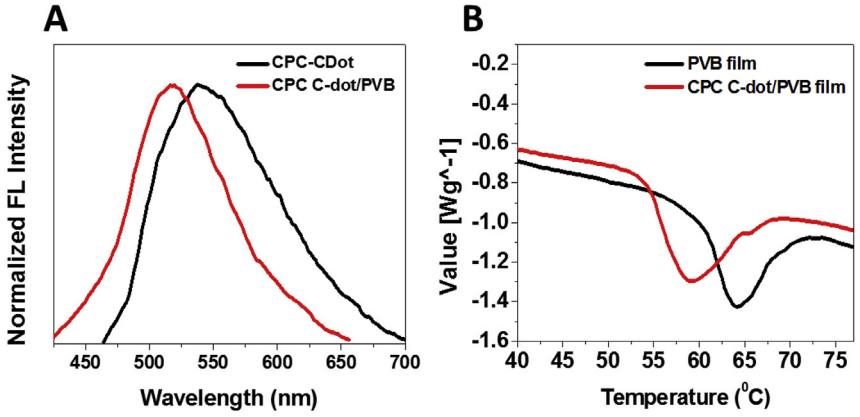

Fig. 3. Spectroscopic and thermodynamic impact of carbon dot-polymer interactions. (**A**) Excitation-dependent emission spectra of 2 mg/ml CPC C-dots in chloroform solution (black) and CPC C-dot/PVB film (red); (**B**) differential scanning calorimetry (DSC) traces depicting the glass transition temperature (Tg) of 4 mg bare PVB film (black) and 4 mg of CPC C-dot/PVB composite film (red). Traces were measured in air from 30 to 210 °C at a 20 °C/min rate. (A colour version of this figure can be viewed online.)

depicts the visual and spectroscopic relationship between stretching of the C-dot/polymer films and their fluorescence emissions. In the experiments, 2 cm × 0.2 cm films were fabricated and placed between two clamps in a tensile test instrument. The clamps were then gradually pulled apart using a mechanical servo screw drive, producing an increasing strain until the film sample finally tore. During the experiment, the force applied for film stretching was measured as well as the corresponding film elongation. Importantly, the fluorescence appearance and emissions of the films were recorded at each stage of stretching using a conventional spectrofluorimeter (Fig. 4).

The data in Fig. 4 demonstrate remarkable fluorescence transformations of the C-dot/PVB films that were directly correlated to the extent of film stretching. Fig. 4A, for example, shows that the CPC-C-dot/PVB film changed from a diminished green color prior to stretching to intense green-blue appearance upon stretching to 265% with respect to the initial film length. Similarly, the DAAQ-C-dot/PVB film appeared dark orange-red in its un-stretched state, transforming into bright orange in the highly stretched (265%) condition (Fig. 4B).

The spectral analysis in Fig. 4 (right) further underscores the dramatic tensile-dependent modulation of the films' fluorescence

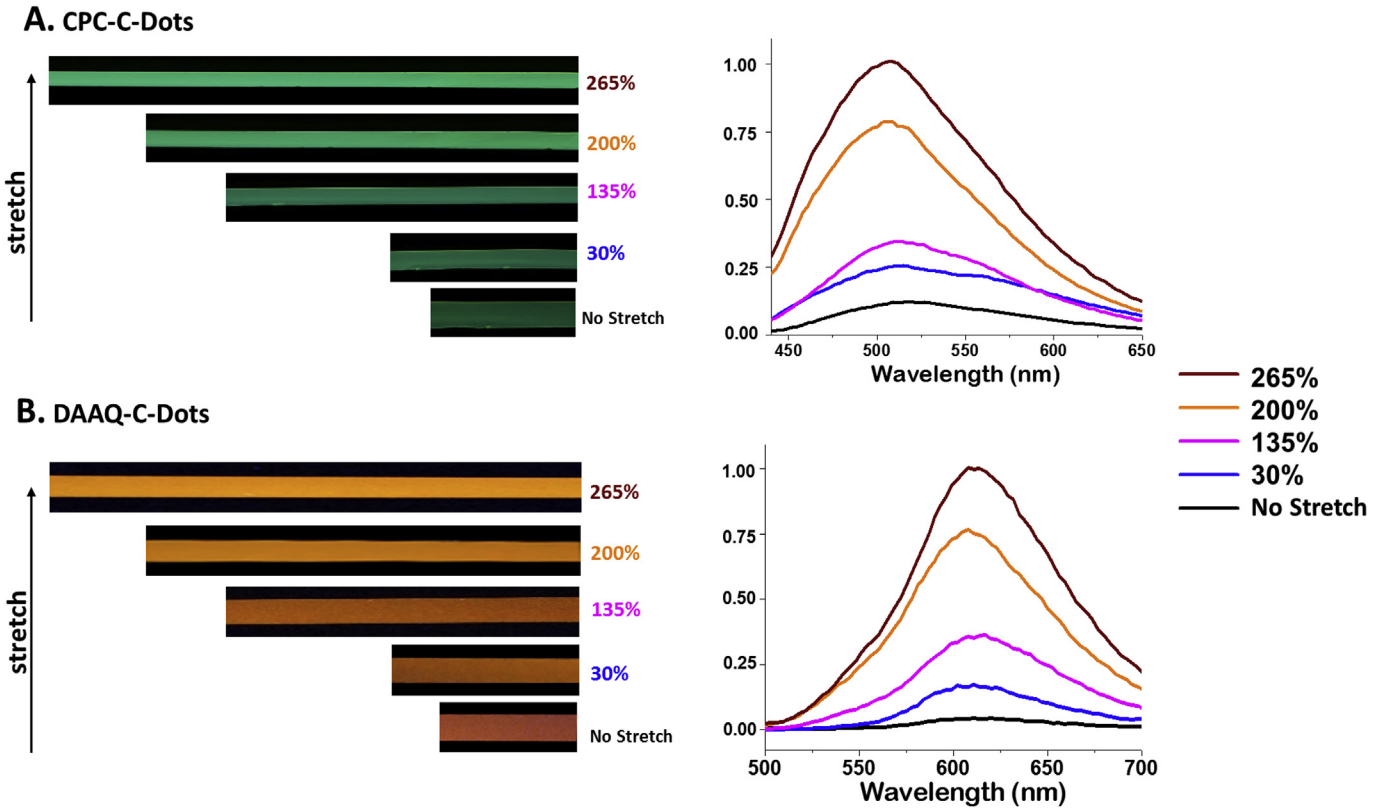

Fig. 4. Stretch-dependent fluorescence transformations of the carbon-dot/PVB films. (**A**) Fluorescence photographs of a CPC-C-dot/PVB film at different tensile strengths. The degree of film stretching (beyond the initial film length) is indicated in percentage values. The corresponding normalized fluorescence emission spectra (λex = 400 nm) are shown on the right. (**B**) Fluorescence photographs of a Daaq-C-dot/PVB film at different tensile strengths. The degree of film stretching (beyond the initial film length) is indicated in percentage values. The corresponding normalized fluorescence emission spectra (λex = 480 nm) are shown on the right. (A colour version of this figure can be viewed online.)

signals, specifically the pronounced enhancement of the fluorescence emissions upon film elongation. Indeed, in both CPC-C-dot/PVB film and Daaq-C-dot/PVB film, the emission peaks exhibited considerably higher intensities upon film stretching. Moreover, the fluorescence intensity enhancement went hand in hand with blue shifts of the emission peaks; this effect was particularly apparent in case of CPC-C-dot/PVB which shifted from approximately 520 nm prior to stretching, to around 500 nm following elongation of the film by 265% (Fig. 4A). A lesser blue shift, yet still experimentally significant - from around 620 to 610 nm - was also apparent in case of the Daaq-C-dot/PVB film (Fig. 4B). While Fig. 4 demonstrates that the fluorescence intensity of the PVB-embedded C-dots exhibited significant sensitivity to film stretching, we also examined the quantitative relationships between the recorded fluorescence emissions and specific mechanical parameters – film stress and strain [65](Fig. 5). Fig. 5 presents experimental data in which the stress and strain of the C-dot/PVB films were measured upon uniaxial application of a constant strain loading rate of 20 mm/min. In parallel, the fluorescence intensities emitted by the films at specific strain/stress were recorded.

Fig. 5 depicts the relationships between the true-stress (T-stress) and true-strain (T-strain) obtained for the CPC-C-dot/PVB (Fig. 5A) and DAAQ-C-dot/PVB (Fig. 5B) films, and the corresponding fluorescence intensities recorded at specific T-stress/T-strain points. The T-stress and T-strain were obtained according to the following equations [66].

$$T\text{-stress: } \sigma_t = \sigma_e(1 + \varepsilon_e)$$

$$T\text{-strain: } \varepsilon_t = ln(1 + \varepsilon_e)$$

in which σ_e and ε_e are the engineering (experimentally-measured) strain and stress, respectively.

It should be emphasized that T-stress and T-strain were employed here rather than the recorded stress/strain as they better reflect the plasticity of polymer films undergoing stretch deformations [67]. Accordingly, the T-stress/T-strain curves in Fig. 5 reflect the interdependence between film stress and strain, up to the rupture point at high strain values. The curves reflect conventional behaviour of amorphous elastic like polymers rising in an exponential manner as the stress gradually increases with an increase in strain [68,69].

Fig. 5 depicts the T-stress/T-strain curves recorded for the two C-dot/PVB films, obtained at a constant strain rate of 20 mm/min at room temperature, and the corresponding fluorescence intensities (for CPC-C-dot/PVB - $\lambda_{ex} = 400$ nm, maximal emission values at around 520 nm; for Daaq-C-dot/PVB - $\lambda_{ex} = 480$ nm, maximal emission values at around 620 nm). Specifically, as the films were stretched from T-strain of 0–3.4 (corresponding to 0%–265% elongation, i.e. Fig. 3), the T-stress exponentially increased from 0 to 60 MPa. Fig. 5 reveals remarkable quantitative correlations between the fluorescence intensities of the films (recorded at distinct film elongation points corresponding to different strains) and the mechanical parameters pertaining to film stretching (T-strain/T-stress curves, and calculated T-stress). The correlation between fluorescence emission intensity and strain/stress values was apparent for both CPC-C-dot/PVB film (Fig. 5A), and the DAAQ-C-dot/PVB film (Fig. 5B).

An important result in Fig. 5 is that in both C-dot/PVB films the fluorescence intensities of the C-dots exhibit exponential enhancement upon T-strain increase, closely tracing the calculated

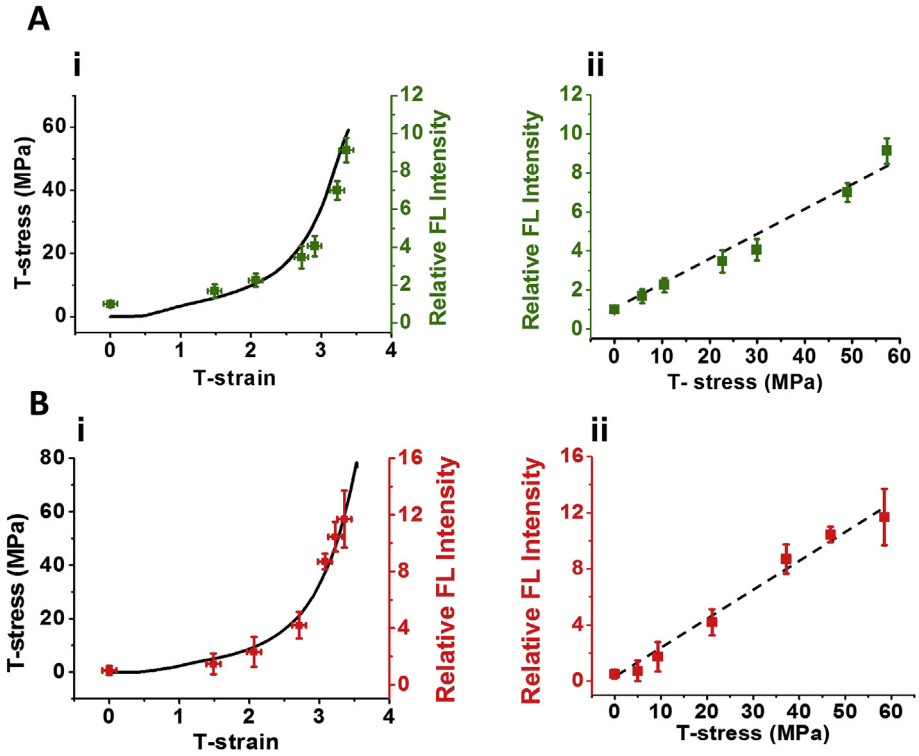

Fig. 5. Correlation between fluorescence intensity and stress/strain of the carbon-dot/PVB films. (**A**) CPC-C-dot/PVB; (**B**) Daaq-C-dot/PVB. (**i**) Tensile true stress (T-stress)/true strain (T-strain) curves recorded at strain rates of 20 mm/min (black lines). The Tensile T-stress/T-strain curve is correlated to the fluorescence intensities (relative to the non-stretched films in which the fluorescence emission was defined as "1"; green values correspond to CPC-C-dot/PVB and red points account for Daaq-C-dot/PVB). (**ii**) Correlation between the fluorescence intensities of the C-dot/PVB films and the measured T-stress. The black lines correspond to the linear fittings. (A colour version of this figure can be viewed online.)

T-stress curves. The exponential behaviour of the fluorescence/strain relationship is depicted in Figs. 9 and SI. This remarkable correlation is likely due to the fact that during plastic deformation, the entangled polymer chains undergo moderate relaxation upon strain increase, resulting in small enhancement in stress [70], which, in turn, yields less pronounced separation of the polymer-embedded C-dots and concomitant small enhancement of fluorescence intensity (Fig. 5). However, following the relaxation stage, strain-induced chain reorientation along the tensile axis requires significantly greater work accounting for the steep increase in stress [71]. Chain reorientation gives rise to significant separation among the PVB-embedded C-dots, accounting for the precipitous enhancement of fluorescence intensity, which nicely correlates with the stress increase (Fig. 5). The remarkable correlation between the strain/stress curves and fluorescence emission intensity attest to the interdependence between the mechanical properties of the films and C-dots' chemical environment, particularly the average distances among the C-dots which affect the degree of fluorescence quenching/de-quenching [72]. Supporting this interpretation is an experiment in which lower concentrations of C-dots were detected in the same film volumes extracted from differently-stretched films (Figs. 10 and SI).

Particularly striking is the almost linear relationship between the relative fluorescence emission peaks of the composite C-dot/PVB films, and the calculated T-stress (Fig. 5A,ii for CPC-C-dot/PVB and Fig. 5B,ii for DAAQ-C-dot/PVB). The linearity is manifested in the high R^2 factor of above 0.98 for both films. The linear relationship between film fluorescence and mechanical stress (Fig. 5A,ii and Fig. 5B,ii) essentially constitutes an effective "calibration curve", allowing accurate stress determination based upon recording the C-dot/polymer film fluorescence. Overall, the data in Fig. 5 demonstrate an extraordinary quantitative correlation between the fluorescence of the C-dot/PVB composites and the intrinsic mechanical properties of the films.

3.4. Optical applications of the stretch-dependent fluorescent C-dot/PVB films

The dependence of the C-dot/PVB fluorescence upon mechanical modulation of the composite films, particularly its stretching, facilitated interesting optical applications. Fig. 6 demonstrates generation of mechanically-tuneable white light emission upon

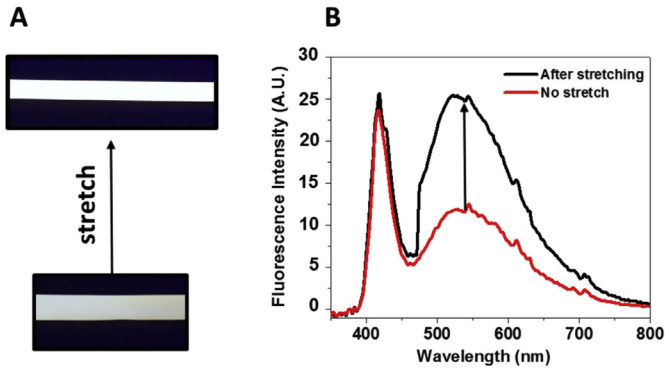

Fig. 6. Mechano-optical modulation using a mixed carbon-dot/PVB film. (**A**) Photographs of a mixed C-dot/PVB composite film at two stretching states using $\lambda = 410$ nm light emitting diode (LED). (**B**) Corresponding photoluminescence spectra of the film prior to stretching (red) and after stretching (black). (A colour version of this figure can be viewed online.)

illuminating a PVB film hosting both CPC-C-dots and Daaq-C-dots with a blue (410 nm) light emitting diode (LED), while simultaneously stretching the film. As apparent in the photographs shown in Fig. 6A, the transparent film was initially (prior to stretching) whitish-grey and exhibited low intensity; however, following 50% stretching, the film emitted intense white light (Fig. 6A). This remarkable phenomenon is due to the combined enhanced fluorescence emissions of the two C-dot species interspersed within the PVB matrix – green in case of CPC-C-dots and red for Daaq-C-dots. Indeed, the photoluminescence spectrum in Fig. 6B underscores both the spectral profile accounting for the white light emission [73], specifically the broad emission peak from around 450 nm–700 nm, as well as the dramatic stretching-dependent emission enhancement accounting for the greater light intensity. The CIE coordinates of the LED-illuminated stretched film (0.310, 0.353) are shown in Figs. 11 and SI, confirming the white light properties.

4. Conclusions

This work presents a new C-dot/polymer composite allowing quantitative sensing of tensile modulation in elastic films. Specifically, we incorporated C-dots within a PVB host matrix, and demonstrated that the shift, and particularly intensity of the C-dots' fluorescence was intimately linked to stretching of the films. Importantly, we show that the fluorescence emission intensity of the C-dots exhibited excellent correlation to the films' stress and strain, allowing quantitative determination of these parameters. The remarkable mechano-optical modulation of the C-dot/PVB films is attributed to the dependence of C-dots' fluorescence upon the average distance between immobilized particles in a host matrix. Besides fluorescence-based tensile sensing, the C-dot/PVB films were employed for fabricating a novel mechanically-tuneable white light emitter. In conclusion, the tensile-dependent fluorescence of the C-dot/PVB composites represents a unique physicochemical phenomenon having significant technological potential. The C-dot/polymer films exhibit practical advantages, such as readily-available and inexpensive reagents, a simple synthesis scheme, and easily recorded optical output. The concept we introduce is generic and can be implemented in sensing and optical applications using varied C-dots and polymeric matrixes.

Acknowledgments

We are grateful to Dr. Yaakov B. Unigovski (assistance with tensile measurements), Dr. Natalya Froumin (XPS), Dr. Yanna Milionshi (DSC), Dr. Alexander Upcher (TEM), Dr. Ezersky Vladimir (HR-TEM), Jurgen Jopp (AFM), Ms. Orit Malka (Confocal microscopy) and Mr. Ahiud Morag for help with the digital images.

Appendix A. Supplementary data

Supplementary data to this article can be found online at https://doi.org/10.1016/j.carbon.2019.06.046.

References

[1] M. Amjadi, K.U. Kyung, I. Park, M. Sitti, Stretchable, skin-mountable, and wearable strain sensors and their potential applications: a review, Adv. Funct. Mater. 26 (2016) 1678–1698, https://doi.org/10.1002/adfm.201504755.
[2] W. Wu, H. Haick, Materials and wearable devices for autonomous monitoring of physiological markers, Adv. Mater. (2018) 1705024, https://doi.org/10.1002/adma.201705024.
[3] M.M. Caruso, D.A. Davis, Q. Shen, S.A. Odom, N.R. Sottos, S.R. White, J.S. Moore, Mechanically-induced chemical changes in polymeric materials, Chem. Rev. 109 (2009) 5755–5798, https://doi.org/10.1021/cr9001353.
[4] Y. Yang, M.W. Urban, Self-healing polymeric materials, Chem. Soc. Rev. 42 (2013) 7446–7467, https://doi.org/10.1039/c3cs60109a.
[5] J. Wang, J.A. Kaplan, Y.L. Colson, M.W. Grinstaff, Mechanoresponsive materials for drug delivery: harnessing forces for controlled release, Adv. Drug Deliv. Rev. 108 (2017) 68–82, https://doi.org/10.1016/j.addr.2016.11.001.
[6] T. Sekitani, H. Nakajima, H. Maeda, T. Fukushima, T. Aida, K. Hata, T. Someya, Diode display using printable elastic conductors, Nat. Mater. 8 (2009) 494–499, https://doi.org/10.1038/nmat2459.
[7] S. Xu, Y. Zhang, X. Li, J. Zhang, J. Sun, L. Cheng, B. Chen, Remarkable fluorescence enhancement of upconversion composite film and its application on mercury sensing, J. Rare Earths 35 (2017) 460–467, https://doi.org/10.1016/S1002-0721(17)60934-7.
[8] Y. Kim, J. Zhu, B. Yeom, M. Di Prima, X. Su, J.G. Kim, S.J. Yoo, C. Uher, N.A. Kotov, Stretchable nanoparticle conductors with self-organized conductive pathways, Nature 500 (2013) 59–63, https://doi.org/10.1038/nature12401.
[9] C. Minnai, M. Di Vece, P. Milani, Mechanical-optical-electro modulation by stretching a polymer-metal nanocomposite, Nanotechnology 28 (2017), https://doi.org/10.1088/1361-6528/aa7c07.
[10] A. Pucci, G. Ruggeri, Mechanochromic polymer blends, J. Mater. Chem. 21 (2011) 8282–8291, https://doi.org/10.1039/c0jm03653f.
[11] M. Drack, I. Graz, T. Sekitani, T. Someya, M. Kaltenbrunner, S. Bauer, An imperceptible plastic electronic wrap, Adv. Mater. 27 (2014) 34–40, https://doi.org/10.1002/adma.201403093.
[12] F. Yin, D. Ye, C. Zhu, L. Qiu, Y.A. Huang, Stretchable, highly durable ternary nanocomposite strain sensor for structural health monitoring of flexible aircraft, Sensors (2017) 17, https://doi.org/10.3390/s17112677.
[13] T. Yamada, Y. Hayamizu, Y. Yamamoto, Y. Yomogida, A. Izadi-Najafabadi, D.N. Futaba, K. Hata, A stretchable carbon nanotube strain sensor for human-motion detection, Nat. Nanotechnol. 6 (2011) 296–301, https://doi.org/10.1038/nnano.2011.36.
[14] S. Zhao, J. Li, D. Cao, G. Zhang, J. Li, K. Li, Y. Yang, W. Wang, Y. Jin, R. Sun, C.P. Wong, Recent advancements in flexible and stretchable electrodes for electromechanical sensors: strategies, materials, and features, ACS Appl. Mater. Interfaces 9 (2017) 12147–12164, https://doi.org/10.1021/acsami.6b13800.
[15] C. Li, D. Zhang, C. Deng, P. Wang, Y. Hu, Y. Bin, Z. FAN, L. Pan, High performance strain sensor based on buckypaper for full-range detection of human motions, Nanoscale (2018), https://doi.org/10.1039/C8NR02196A.
[16] Z. Sang, K. Ke, I. Manas-zloczower, Interface design strategy for the fabrication of highly stretchable strain sensors, ACS Appl. Mater. Interfaces 10 (2018) 36483–36492, https://doi.org/10.1021/acsami.8b14573.
[17] J. Shieh, J.E. Huber, N.A. Fleck, M.F. Ashby, The selection of sensors, Prog. Mater. Sci. 46 (2001) 461–504, https://doi.org/10.1016/S0079-6425(00)00011-6.
[18] C. Neumann, S. Reichardt, P. Venezuela, M. Drögeler, L. Banszerus, M. Schmitz, K. Watanabe, T. Taniguchi, F. Mauri, B. Beschoten, S.V. Rotkin, C. Stampfer, Raman spectroscopy as probe of nanometre-scale strain variations in graphene, Nat. Commun. 6 (2015) 1–7, https://doi.org/10.1038/ncomms9429.
[19] A. Pawlak, A. Galeski, Determination of stresses around beads in stressed epoxy resin by photoelasticity, J. Appl. Polym. Sci. 86 (2002) 1436–1444, https://doi.org/10.1002/app.11299.
[20] Z. Qiu, W. Zhao, M. Cao, Y. Wang, J.W.Y. Lam, Z. Zhang, X. Chen, B.Z. Tang, Dynamic visualization of stress/strain distribution and fatigue crack propagation by an organic mechanoresponsive aie luminogen, Adv. Mater. 1803924 (2018) 1–8, https://doi.org/10.1002/adma.201803924.
[21] F. Ciardelli, G. Ruggeri, A. Pucci, Dye-containing polymers: methods for preparation of mechanochromic materials, Chem. Soc. Rev. 42 (2013) 857–870, https://doi.org/10.1039/c2cs35414d.
[22] C. Calvino, L. Neumann, C. Weder, S. Schrettl, Approaches to polymeric mechanochromic materials, J. Polym. Sci. A Polym. Chem. 55 (2017) 640–652, https://doi.org/10.1002/pola.28445.
[23] R. Klajn, Spiropyran-based dynamic materials, Chem. Soc. Rev. 43 (2014) 148–184, https://doi.org/10.1039/c3cs60181a.
[24] S.F. Yin, Z.M. Zhao, W.L. Luan, S.T. Tu, In-situ strain gauge: based on photoluminescence of quantum dots, Proc. Eng. 130 (2015) 1788–1794, https://doi.org/10.1016/j.proeng.2015.12.335.
[25] C. Minnai, P. Milani, Metal-polymer nanocomposite with stable plasmonic tuning under cyclic strain conditions, Appl. Phys. Lett. 107 (2015), https://doi.org/10.1063/1.4928725.
[26] B.R. Crenshaw, C. Weder, Deformation-induced color changes in melt-processed photoluminescent polymer blends, Chem. Mater. 15 (2003) 4717–4724, https://doi.org/10.1021/cm034447t.
[27] Y. Sagara, S. Yamane, M. Mitani, C. Weder, T. Kato, Mechanoresponsive luminescent molecular assemblies: an emerging class of materials, Adv. Mater. 28 (2016) 1073–1095, https://doi.org/10.1002/adma.201502589.
[28] X. Li, S. Zhu, B. Xu, K. Ma, J. Zhang, B. Yang, W. Tian, Self-assembled graphene quantum dots induced by cytochrome c: a novel biosensor for trypsin with remarkable fluorescence enhancement, Nanoscale 5 (2013) 7776–7779, https://doi.org/10.1039/c3nr00006k.
[29] S. Bhattacharya, S. Nandi, R. Jelinek, Carbon-dot-hydrogel for enzyme-mediated bacterial detection, RSC Adv. 7 (2017) 588–594, https://doi.org/10.1039/c6ra25148j.
[30] S. Bhattacharya, R. Sarkar, B. Chakraborty, A. Porgador, R. Jelinek, Nitric oxide sensing through azo-dye formation on carbon dots, ACS Sens. 2 (2017) 1215–1224, https://doi.org/10.1021/acssensors.7b00356.
[31] S.K. Bhunia, S. Dolai, H. Sun, R. Jelinek, "On/off/on" hydrogen-peroxide sensor

with hemoglobin-functionalized carbon dots, Sensor. Actuator. B Chem. 270 (2018) 223–230, https://doi.org/10.1016/j.snb.2018.05.029.
[32] Y. Song, S. Zhu, B. Yang, Bioimaging based on fluorescent carbon dots, RSC Adv. 4 (2014) 27184–27200, https://doi.org/10.1039/c3ra47994c.
[33] J. Zhang, S.H. Yu, Carbon dots: large-scale synthesis, sensing and bioimaging, Mater. Today 19 (2016) 382–393, https://doi.org/10.1016/j.mattod.2015.11.008.
[34] S. Nandi, M. Ritenberg, R. Jelinek, Bacterial detection with amphiphilic carbon dots, Analyst 140 (2015) 4232–4237, https://doi.org/10.1039/c5an00471c.
[35] T. Feng, Q. Zeng, S. Lu, X. Yan, J. Liu, S. Tao, M. Yang, B. Yang, Color-tunable carbon dots possessing solid-state emission for full-color light-emitting diodes applications, ACS Photonics 5 (2018) 502–510, https://doi.org/10.1021/acsphotonics.7b01010.
[36] R. Jelinek, Carbon Quantum Dots, 2017, https://doi.org/10.1007/978-3-319-43911-2.
[37] Q. Fang, Y. Dong, Y. Chen, C.H. Lu, Y. Chi, H.H. Yang, T. Yu, Luminescence origin of carbon based dots obtained from citric acid and amino group-containing molecules, Carbon 118 (2017) 319–326, https://doi.org/10.1016/j.carbon.2017.03.061.
[38] K. Hola, A.B. Bourlinos, O. Kozak, K. Berka, K.M. Siskova, M. Havrdova, J. Tucek, K. Safarova, M. Otyepka, E.P. Giannelis, R. Zboril, Photoluminescence effects of graphitic core size and surface functional groups in carbon dots: COO-induced red-shift emission, Carbon 70 (2014) 279–286, https://doi.org/10.1016/j.carbon.2014.01.008.
[39] V. Strauss, J.T. Margraf, C. Dolle, B. Butz, T.J. Nacken, J. Walter, W. Bauer, W. Peukert, E. Spiecker, T. Clark, D.M. Guldi, Carbon nanodots: toward a comprehensive understanding of their photoluminescence, J. Am. Chem. Soc. 136 (2014) 17308–17316, https://doi.org/10.1021/ja510183c.
[40] K. Jiang, S. Sun, L. Zhang, Y. Lu, A. Wu, C. Cai, H. Lin, Red, green, and blue luminescence by carbon dots: full-color emission tuning and multicolor cellular imaging, Angew. Chem. Int. Ed. 54 (2015) 5360–5363, https://doi.org/10.1002/anie.201501193.
[41] X. Sun, Y. Lei, Fluorescent carbon dots and their sensing applications, Trac. Trends Anal. Chem. 89 (2017) 163–180, https://doi.org/10.1016/j.trac.2017.02.001.
[42] Y. Liu, P. Wang, K.A. Shiral Fernando, G.E. Lecroy, H. Maimaiti, B.A. Harruff-Miller, W.K. Lewis, C.E. Bunker, Z.L. Hou, Y.P. Sun, Enhanced fluorescence properties of carbon dots in polymer films, J. Mater. Chem. C 4 (2016) 6967–6974, https://doi.org/10.1039/c6tc01932c.
[43] S.K. Bhunia, S. Nandi, R. Shikler, R. Jelinek, Tuneable light-emitting carbon-dot/polymer flexible films prepared through one-pot synthesis, Nanoscale 8 (2016) 3400–3406, https://doi.org/10.1039/c5nr08400h.
[44] B. Zheng, T. Liu, M.C. Paau, M. Wang, Y. Liu, L. Liu, C. Wu, J. Du, D. Xiao, M.M.F. Choi, One Pot Selective Synthesis of Water and Organic Soluble Carbon Dots with Green Fluorescence Emission †, 2015, https://doi.org/10.1039/c4ra16529b.
[45] C. Gooijer, An Introduction to fluorescence spectroscopy, Anal. Chim. Acta 419 (2000) 116–117, https://doi.org/10.1016/S0026-265X(00)00048-5.
[46] S. Bhattacharya, R.S. Phatake, S. Nabha Barnea, N. Zerby, J.J. Zhu, R. Shikler, N.G. Lemcoff, R. Jelinek, Fluorescent self-healing carbon dot/polymer gels, ACS Nano (2019), https://doi.org/10.1021/acsnano.8b07087.
[47] M. Suchitra, Thermal analysis of composites using DSC, Adv. Topics Char. Compos. (2004) 11–33.
[48] S.R. Shi, M.E. Key, K.L. Kalra, Antigen retrieval in formalin-fixed, paraffin-embedded tissues: an enhancement method for immunohistochemical staining based on microwave oven heating of tissue sections, J. Histochem. Cytochem. 39 (1991) 741–748, https://doi.org/10.1177/39.6.1709656.
[49] D. American Society for Testing Materials, 882: standard test method for tensile properties of thin plastic sheeting, Astm 14 (2002) 1–10.
[50] X. Zhang, Y. Shi, H. Hao, J. Cui, The mechanical properties of Polyvinyl Butyral (PVB) at high strain rates, Constr. Build. Mater. 93 (2015) 404–415, https://doi.org/10.1016/j.matdes.2015.06.076.
[51] W. Liu, C. Li, Y. Ren, X. Sun, W. Pan, Y. Li, J. Wang, W. Wang, Carbon dots: surface engineering and applications, J. Mater. Chem. B 4 (2016) 5772–5788, https://doi.org/10.1039/c6tb00976j.
[52] S. Kumar Bhunia, S. Nandi, R. Shikler, R. Jelinek, Tuneable light-emitting carbon-dot/polymer flexible films prepared through one-pot synthesis †, Nanoscale 8 (2016) 3400, https://doi.org/10.1039/c5nr08400h.
[53] S. Lin, C. Lin, M. He, R. Yuan, Y. Zhang, Y. Zhou, W. Xiang, X. Liang, Solvatochromism of bright carbon dots with tunable long-wavelength emission from green to red and their application as solid-state materials for warm WLEDs, RSC Adv. 7 (2017) 41552–41560, https://doi.org/10.1039/c7ra07736j.
[54] J. Tang, B. Kong, H. Wu, M. Xu, Y. Wang, Y. Wang, D. Zhao, G. Zheng, Carbon nanodots featuring efficient FRET for real-time monitoring of drug delivery and two-photon imaging, Adv. Mater. 25 (2013) 6569–6574, https://doi.org/10.1002/adma.201303124.
[55] J. Tian, Y. Leng, Z. Zhao, Y. Xia, Y. Sang, P. Hao, J. Zhan, M. Li, H. Liu, Carbon quantum dots/hydrogenated TiO2nanobelt heterostructures and their broad spectrum photocatalytic properties under UV, visible, and near-infrared irradiation, Nano Energy 11 (2015) 419–427, https://doi.org/10.1016/j.nanoen.2014.10.025.
[56] O. Ej, K. Kozak, K. Kumara, R. Datta, M. Greplova, G. Vaclav, V. Ranc, J. Kas, R. Zbor, Surfactant-derived Amphiphilic Carbon Dots with Tunable Photoluminescence, 2013, https://doi.org/10.1021/jp4040166.
[57] W. Zhou, J. Zhuang, W. Li, C. Hu, B. Lei, Y. Liu, Towards efficient dual-emissive carbon dots through sulfur and nitrogen co-doped, J. Mater. Chem. C 5 (2017) 8014–8021, https://doi.org/10.1039/c7tc01819c.
[58] T. Zhang, J. Zhu, Y. Zhai, H. Wang, X. Bai, B. Dong, H. Wang, H. Song, A novel mechanism for red emission carbon dots: hydrogen bond dominated molecular states emission, Nanoscale 9 (2017) 13042–13051, https://doi.org/10.1039/C7NR03570E.
[59] G. Yang, X. Wan, Y. Liu, R. Li, Y. Su, X. Zeng, J. Tang, Luminescent poly(vinyl alcohol)/carbon quantum dots composites with tunable water-induced shape memory behavior in different pH and temperature environments, ACS Appl. Mater. Interfaces 8 (2016) 34744–34754, https://doi.org/10.1021/acsami.6b11476.
[60] Y. Chen, H. Lian, Y. Wei, X. He, Y. Chen, B. Wang, Q. Zeng, J. Lin, Concentration-induced multi-colored emissions in carbon dots: origination from triple fluorescent centers, Nanoscale 10 (2018) 6734–6743, https://doi.org/10.1039/c8nr00204e.
[61] M. Schmid, S. Affolter, Interlaboratory tests on polymers by differential scanning calorimetry (DSC): determination and comparison of oxidation induction time (OIT) and oxidation induction temperature (OIT), Polym. Test. 22 (2003) 419–428, https://doi.org/10.1016/S0142-9418(02)00122-8.
[62] S. Bhuvana, M. Prabakaran, Synthesis and characterisation of polyamide/halloysite nanocomposites prepared by solution intercalation method, Nanosci. Nanotechnol. 4 (2014) 44–51, https://doi.org/10.5923/j.nn.20140403.02.
[63] A. Karatrantos, N. Clarke, R.J. Composto, K.I. Winey, Entanglements in polymer nanocomposites containing spherical nanoparticles, Soft Matter 12 (2016) 2567–2574, https://doi.org/10.1039/c5sm02010g.
[64] C.E. Corcione, M. Frigione, Characterization of nanocomposites by thermal analysis, Materials 5 (2012) 2960–2980, https://doi.org/10.3390/ma5122960.
[65] F. Cellini, S. Khapli, S.D. Peterson, M. Porfiri, Mechanochromic polyurethane strain sensor, Appl. Phys. Lett. 105 (2014), https://doi.org/10.1063/1.4893010.
[66] D. Roylance, Stress-strain Curves, 2001, pp. 1–14.
[67] Y. Song, K.H. Nitta, N. Nemoto, Molecular orientations and true stress-strain relationship in isotactic polypropylene film, Macromolecules 36 (2003) 8066–8073, https://doi.org/10.1021/ma030194d.
[68] H.J. Qi, M.C. Boyce, Stress-strain Behavior of Thermoplastic Polyurethane, 2004, pp. 1–51.
[69] L. Bohan, S. Yueting, L. Yibing, W. Yan, G. Dongyun, X. Jun, Systematic experimental study on mechanical behavior of PVB (polyvinyl butyral) material under various loading conditions, Polym. Eng. Sci. 52 (5) (2012) 1137.
[70] R.S. Porter, J.F. Johnson, The entanglement concept in polymer systems, Chem. Rev. 66 (1966) 1–27, https://doi.org/10.1021/cr60239a001.
[71] M.F. Milagin, N.I. Shishkin, Change in the molecular orientation in highly elastically stretched amorphous polymers, Polym. Sci. 30 (1988) 2398–2404, https://doi.org/10.1016/0032-3950(88)90002-0.
[72] Y. Chen, M. Zheng, Y. Xiao, H. Dong, H. Zhang, J. Zhuang, H. Hu, B. Lei, Y. Liu, A self-quenching-resistant carbon-dot powder with tunable solid-state fluorescence and construction of dual-fluorescence morphologies for white light-emission, Adv. Mater. 28 (2016) 312–318, https://doi.org/10.1002/adma.201503380.
[73] F. Zhang, X. Feng, Y. Zhang, L. Yan, Y. Yang, X. Liu, Photoluminescent carbon quantum dots as a directly film-forming phosphor towards white LEDs, Nanoscale 8 (2016) 8618–8632, https://doi.org/10.1039/c5nr08838k.